

Influence of different dry-mixing techniques on the mechanical, thermal, and electrical behavior of ultra-high molecular weight polyethylene/exhausted tire carbon composites

Original

Influence of different dry-mixing techniques on the mechanical, thermal, and electrical behavior of ultra-high molecular weight polyethylene/exhausted tire carbon composites / Duraccio, Donatella; Arrigo, Rossella; Bartoli, Mattia; Paolo Capra, Pier; Malucelli, Giulio. - In: POLYMERS FOR ADVANCED TECHNOLOGIES. - ISSN 1042-7147. - ELETTRONICO. - (2022), pp. 1-10. [10.1002/pat.5637]

Availability:

This version is available at: 11583/2956078 since: 2022-09-08T15:58:13Z

Publisher:

Wiley

Published

DOI:10.1002/pat.5637

Terms of use:

This article is made available under terms and conditions as specified in the corresponding bibliographic description in the repository

Publisher copyright

Wiley postprint/Author's Accepted Manuscript

This is the peer reviewed version of the above quoted article, which has been published in final form at <http://dx.doi.org/10.1002/pat.5637>. This article may be used for non-commercial purposes in accordance with Wiley Terms and Conditions for Use of Self-Archived Versions.

(Article begins on next page)

Influence of different dry-mixing techniques on the mechanical, thermal and electrical behavior of ultra high molecular weight polyethylene/exhausted tire carbon composites

Donatella Duraccio ¹, Rossella Arrigo ², Mattia Bartoli ³, Pier Paolo Capra⁴, Giulio Malucelli ²

¹ Institute of Sciences and Technologies for Sustainable Energy and Mobility, National Council of Research, Strada delle Cacce 73, 10135 Torino, Italy

² Department of Applied Science and Technology, Politecnico di Torino, Viale Teresa Michel 5, 15121 Alessandria, Italy

³ Center for Sustainable Future Technologies, Italian Institute of Technology, Via Livorno 60, 10144 Torino, Italy

⁴ National Institute of Metrological Research (INRIM), Strada delle Cacce 91, 10135, Torino, Italy

Corresponding author: donatella.duraccio@stems.cnr.it

Abstract

The mechanical, thermal and electrical behavior of ultra high molecular weight (UHMWPE) composites containing different amount of pyrolyzed exhausted tire carbon (ETC) is investigated. Composites were obtained by dry-mixing the powders with a homogenizer and an impact mill. The results clearly indicate that, by changing the mixing method, it is possible to tune the rheological and morphological characteristics of the composites and in turn their mechanical, thermal and electrical properties. Better performances were observed for the composites obtained with the impact mill, which showed improved Young modulus, reduced electrical and thermal resistance with respect to those of homogenized counterparts. All the composites exhibited a relevant reduction of electrical resistivity with a percolation threshold of 1.51 vol.%.

Keywords

Exhausted tires, ultra high molecular weight, polymer composites, pyrolysis, mechanical properties, electrical properties

Introduction

Global warming, depletion of fossil fuel and availability of waste materials are key-factors in the development of waste valorization processes. Among others, exhausted tire (ET) disposal represents a serious pollution problem due to the dangerous impact on the environment and human health ^{1,2} so that in all of European area tires landfilling has been forbidden.

The relevant production of this commodity that has led to the accumulation of millions of end-life tires per year and their challenge in recyclability, because of their resistance to harsh mechanical and weather conditions, have exacerbated the problem and nowadays, about 66% of exhausted tires is confined in landfill (outside Europe) or incinerated ³.

A smaller part of the tires is recovered through industrial process for raw materials recycling (i.e. as inert filler for asphalt ⁴ and construction ^{5,6}, for the production of textile materials ⁷ and rubber ⁸⁻¹⁰), for gasification and pyrolysis. These thermochemical routes are cost-effective approaches for end-life tires management and provide an interesting opportunity with a view to a “zero waste” circular economy ^{11,12}.

In this field, pyrolysis is recognized as efficient method for waste valorization ^{13,14} with the simultaneous production of combustible gas, hydrocarbon mixtures and carbon. The literature on this process applied to ET has been widely surveyed. Numerous reports analyzed the advantages and disadvantages of the ET pyrolysis process with respect to other thermochemical approaches ¹⁵⁻¹⁷. The main advantages include both the minor environmental impact (the volume of the output gases from a pyrolysis is smaller than that obtained from combustion process ^{18,19} and the recovery of liquid and solid materials.

However, the current ET pyrolysis is mainly studied for research purposes and it is not yet industrially widespread for several reasons, namely: i) the public acceptance discouraged by the EU legislative barriers that classified this process as incineration; ii) the difficulty of transferring the heat in an efficient way, ensuring uniform distribution during the process; iii) the absence of a wide market mainly for the solid fraction. The solid char (i.e. exhausted tire carbon-ETC) has a very complex composition²⁰ and mainly contains the original carbon black, inorganic compounding fillers and carbonaceous deposits. It has been improperly defined pyrolyzed carbon black though its surface chemistry is very different from that of virgin carbon black²¹.

Up to now, it has been mostly used for the preparation of activated carbons both by physical (steam and CO₂) and chemical activation (using H₂SO₄, KOH, H₃PO₄) for the removal of organic/inorganic pollutants from industrial wastewater and air²². Another possible use is for the development of doped carbon-based electrodes for Li and Na-ion batteries²³⁻²⁵, for electrocatalysts^{26,27} and for supercapacitors^{27,28}.

However, only few papers report on the use of ETC as a filler for the preparation of polymer composites. In this context, it has been used for the preparation of rubber composites^{20,21,29} to be reused in tire formulation and of epoxy nanocomposites for coating applications³⁰. Considering that the demand for using polymer composites in various application areas is vast and that the incorporation of ETC in a solid market is challenging¹³, further studies are required to overcome the barriers behind the incorporation of ETC into polymer composites and giving a positive impact to the sustainability.

In this light, we have prepared ultra high molecular weight polyethylene (UHMWPE)-based ETC composites, in order to assess the effect of the filler on the mechanical, thermal and electrical properties of the polymer matrix. Two techniques were employed for mechanically mixing the powder components, i.e. a homogenizer and a home-made impact mill; the mixing step was followed by compression molding. Characterization was completed by means of rheological study, and scanning electron and optical microscopy. UHMWPE has been selected because it is largely exploited

for a huge variety of industrial applications, thanks to its properties, processability and low cost ³¹. Besides, the interest in UHMWPE-based composites containing carbonaceous fillers is steadily increasing, particularly referring to the design of new conductive polymer composites. Different carbon-based fillers such as carbon nanotubes ^{32,33} and graphene ^{34,35} have been already employed for preparing UHMWPE-composites.

On the other hand, these materials are expensive and non-sustainable and have not fulfilled yet the promise for a new carbon era; therefore, there is an increasing interest in exploiting ETC as a cheap and sustainable alternative to these carbonaceous fillers, in the same way as it is reported for composites containing carbon derived from thermochemical treatment of biomasses (i.e. biochar) ³⁶⁻³⁸.

2. Materials and Methods

2.1 Materials

UHMWPE (Celanese Diversified Chemical Co., China) has a molecular weight of 9×10^6 g mol⁻¹ and average particle size of ~100 μm.

The starting ETC was obtained through pyrolysis of an exhausted tire (Bridgestone branch). The exhausted tire was chopped in small pieces and pyrolyzed in a tubular furnace (Carbolite TZF 12/65/550), operating in nitrogen atmosphere (flux of up 4 mL/min) and using a heating rate of 15 °C/min and reaching 1000°C and kept at this temperature for 30 min.

ETC was recovered after cooling down the reactor to room temperature and used without any further purification.

2.2 Preparation of composites

Two approaches were employed for mixing the powder components. In the first method, UHMWPE was mechanically mixed with a proper amount of ETC particles by using a homogenizer (120 rpm) at room temperature for 1 hour. In the second one, a home-made impact mill (designed and fabricated at the Energy Department of the Politecnico di Torino, Italy) was used, treating the UHMWPE-ETC

powder mixtures at 8000 rpm for 30s³⁹. After mixing, composites were sliced by compression molding in a Collin P200T press, operating at 160 °C and 20 MPa for a total processing time of 7 min.

The mixing ratios of UHMWPE/ETC (wt./wt.) were 100/0, 99/1, 97/3, 95/5, 90/10 and 80/20. Hereinafter, the composites are coded as PEx_H, PEx_M, where x represents the ETC content; H and M represent the powder mixing process (i.e. homogenizer and impact mill, respectively). Unfilled matrix is coded as PE. The electrical and thermal properties of PE20_H and PE20_M composites were measured, whereas their mechanical and rheological properties were not determined because the high ETC loading prevented the obtainment of suitable specimens through compression molding.

2.3 Characterizations

ETC was analyzed by Raman spectroscopy using a Renishaw® Ramanscope InVia (H43662 model, Gloucestershire, UK) equipped with a laser light source with a wavelength of 532 nm. Signals were fitted according to methodology proposed by Tagliaferro et al.⁴⁰.

Density was estimated by compressing a weighted amount of ETC using a hydraulic press (Specac Atlas Manual Hydraulic Press 15T) in non-deformable cylinder of known geometry with a modified set-up based on that reported by Giorcelli et al.⁴¹. A pressure of 1500 bar was applied for 10 min and density was calculated afterwards.

The morphology of the ETC particles was also investigated by means of a field emission scanning electrical microscopy (FE-SEM, Zeis SupraTM 40, Oberkochen, Germany) with a beam voltage of 5kV.

The morphological characterization of the composites was carried out by means of a Zeiss (Oberkochen, Germany) VP Scanning Electron Microscope (beam voltage: 20kV). Before observation, composites were cryogenically fractured in liquid nitrogen and the obtained surfaces were gold metallized, hence making them electrically conductive. Also, a Zeiss MC-80 polarizing optical microscope (POM) (Zeiss, Germany) was used for assessing the morphologies of the

composites in the form of 20- μ m-thick films obtained by compression molding in the conditions described before.

The linear rheological behavior of unfilled polymers and composites was investigated using an ARES (TA Instrument, USA) strain-controlled rheometer equipped with two parallel plates (plate diameter = 25 mm). Frequency sweep measurements were carried out to evaluate the complex viscosity curves in the frequency range between 0.1 and 100 rad/s at 200 °C. The strain amplitude was determined through preliminary strain sweep measurements and was fixed for each sample in order to fall in the linear viscoelastic region. **The gap between the plates was set to 1 mm.**

Tensile tests were performed on compression-molded dumbbell specimens ($50 \times 3.15 \times 1 \text{ mm}^3$) by using an Instron dynamometer (Instron® 5966). According to the ASTM D638-03 standard, for measuring the Young's modulus, the ratio between the drawing rate and the initial length was fixed equal to 0.1 mm/(mm·min); for determining the strain and stress at yield and at break (stress strain curves), the same ratio was selected as 10 mm/(mm·min). Mean values were obtained by averaging over ten independent tests.

A TPS 2500S Hot Disk instrument (AB Corporation-Göteborg, Sweden) was employed for measuring the thermal conductivity of UHMWPE and its composites. The Transient Plane Source (TPS) method⁴² was applied, for which a Kapton sensor (radius 3.189 mm) between two similar slabs of material ($30 \times 30 \times 3 \text{ mm}^3$) was used. The test temperature was set at $23.00 \pm 0.01 \text{ °C}$ and controlled by a silicon oil bath (Haake A40, Thermo Scientific Inc., Waltham, MA USA), equipped with a temperature controller (Haake AC200, Thermo Scientific Inc., Waltham, MA, USA). The thermal conductivity was obtained by the change in temperature recorded when the sensor supplied to the sample a heat pulse of 0.03 W for 2 seconds.

All the DC resistance measurements were performed with a voltamperometric technique in accordance with the ASTM D257 standard method. The samples were placed in a test fixture having a set of three planar electrodes connected to the measurement instruments⁴³. A high DC voltage generator, ranging from 0 to 1000 V, was connected to two of the test fixture electrodes. A pico-

ammeter (model 6517B; Keithley Instruments, Cleveland, Ohio, USA) measured the current that flows through the samples, while the third electrode was connected to a guard voltage generator. The guard voltage reduces the leakage currents that usually occur when measuring high value resistances, thus improving the accuracy and repeatability of the measurement. The measurements were performed at $23.0 \pm 0.3^\circ\text{C}$ by using circular specimens of 6 cm in diameter and 1 mm thick.

3.Results

Figure 1 shows the Raman spectra of ETC collected in the range from 500 cm^{-1} up to 3500 cm^{-1} .

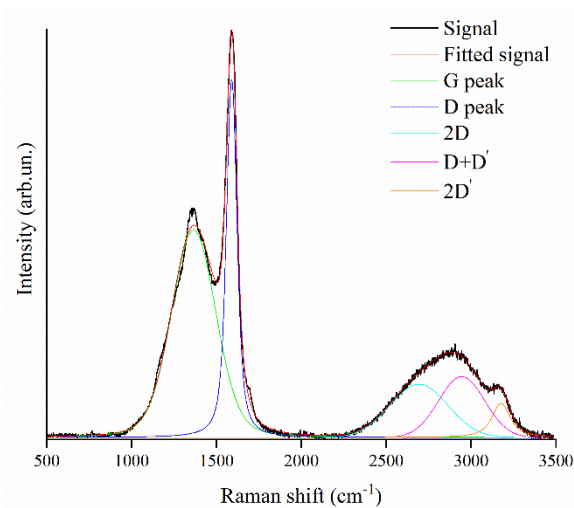


Figure 1. Raman spectra of ETC collected from 500 cm^{-1} up to 3500 cm^{-1} fitted according to Tagliaferro et al. ⁴⁰.

The spectra exhibit a broad intense D band centered at 1366 cm^{-1} and a very narrow G peak centered at 1590 cm^{-1} with an I_D/I_G ratio not exceeding 2.6. This value is significantly higher than others reported for carbon produced at the same temperature ⁴¹ but is in good agreement with the data documented by Tamborrino et al. ⁴⁴. Clearly, ETC is still evolving toward a more graphitic material, passing through a disordered configuration as reported by Ferrari et al. ⁴⁵. This is supported by the not-well resolved structure of the peaks between 2500 and 3500 cm^{-1} , which form a broad band.

FESEM images of virgin ETC show 5-10 μm diameter aggregates (Figure 2 on the left) formed by primary particles (below 100 nm, Figure 2 on the right), with a density of about 1.853 g/cm^3 . The mainly observed shape is the spherical one, due to the carbon black used as filler in the pristine tire, together with the one formed during the cracking of the polymeric matrix. Nevertheless, non-spherical particles are also observed: it is likely that they originated as a consequence of the interaction between polymeric matrix with the other constituents of the tires such as cotton fibers and metal net.

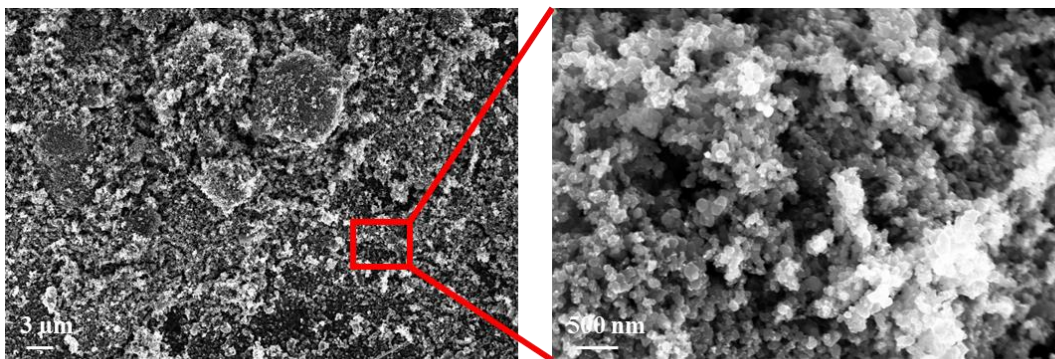


Figure 2. FESEM images of ETC powder at different magnifications. The long range (left) and individual particles (right) morphologies are shown.

By exploiting the light transmittance difference between the polymer and ETC, POM images of UHMWPE/ETC composites (Figure 3) depict the distribution of filler particles (Black lines/regions) at the boundary regions of UHMWPE grains (white regions). This segregated structure, reported in a flurry of works ^{32,34-38} and caused by the high viscosity of the polymer matrix and lack of shear in the composite preparation, is beneficial for the formation of a conductive path.

When the homogenizer is used for mixing the powders, at low ETC content (i.e. 1 wt.%, Figure 3A), filler channels are not very well connected. In PE3_H composites, the network becomes more connected and dense whereas at higher concentration, the ETC region becomes thicker rather than dense, showing with many filler aggregates. A similar behaviour can be observed for the composites obtained by impact mill. However, for this class of composites, the filler channels are already

connected each other when the amount of ETC is 1 wt.% (Figure 3D) and they appear more dense, more uniform in thickness and with a lower amount of aggregated with respect to those displayed in the PE_H composites. As it will be shown later, these findings are well consistent with the electrical resistivity results.

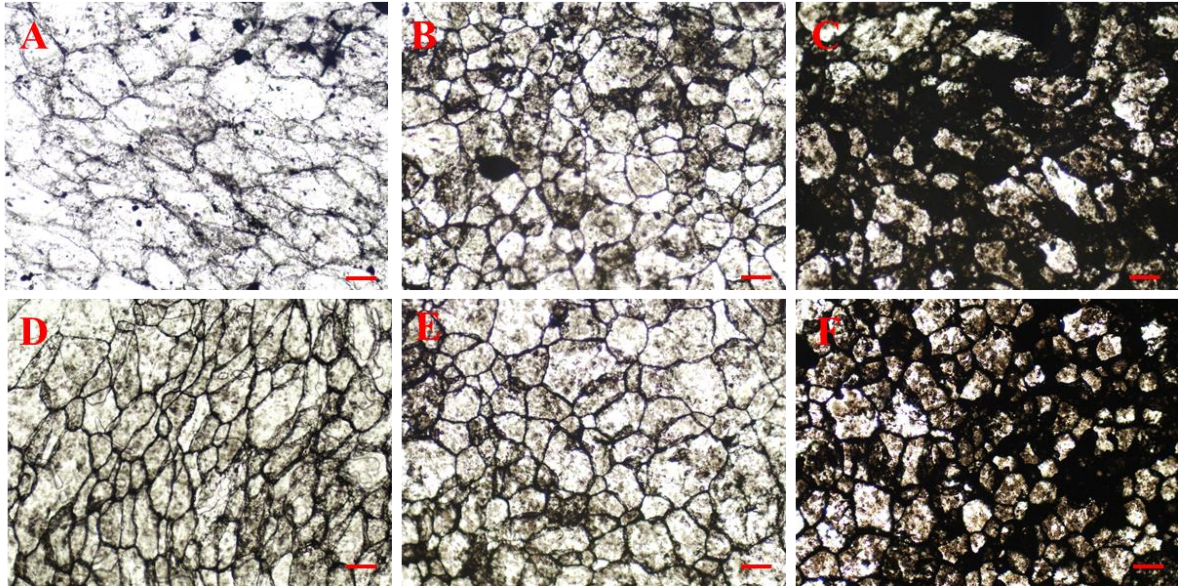


Figure 3. POM images of UHMWPE/ETC composites with different ETC loadings (i.e 1 wt.% (A and D); 3 wt.% (B and E) and 5 wt.% (C and F)) using two different powder mixing procedures (i.e. homogenizer (A, B, C) and impact mill (D, E, F)). The markers correspond to 100 µm length.

Figures 4A and 4B show the cross-section micrographs of PE3_H and PE3_M composites, respectively. In both images, the filler particles are distributed around the perimeter of the original polymer grains. However, in the homogenized composite, the ETC is not well packed as it shows the presence of some holes (evidenced by the white arrow in Fig. 4A). Conversely, using the impact mill, the ETC particles and polymer tightly combine each other. When the ETC concentration is 10 wt.%, the ETC particles completely covered the surface of the original UHMWPE powders and formed a packed network. Nevertheless, the composite obtained by homogenizer presents a less uniform

distribution of filler with respect to the composite obtained by impact mill (Figures 4C-D). In PE10_M, ETC and PE are well inter-dispersed as indicated by the white arrows in Figure 4E.

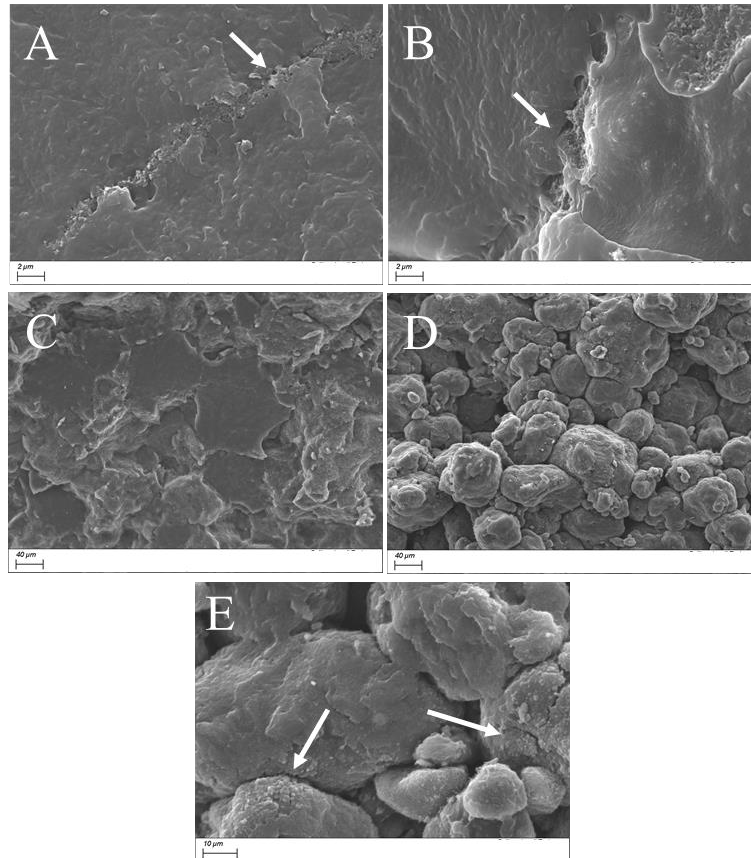


Figure 4. Cross section images of UHMWPE composites containing 3 (A and B) and 10 wt.% of ETC (C, E and D) obtained by homogenizer (A and C) and by impact mill (B, D and E).

Figure 5 reports the complex viscosity **and the storage modulus** as a function of frequency for unfilled UHMWPE and both series of composites. Regardless the used preparation strategy, by increasing the ETC loading, a progressive increase of **both complex viscosity and storage modulus** as compared to the unfilled matrix is observed. This increase is more evident in the low-frequency region. **Besides, the introduction of ETC causes a modification of the UHMWPE rheological behavior from liquid-like to solid-like, as denoted by the flattening of the storage modulus curves of the composites in the low frequency region.** The results clearly indicate that the embedded particles are able to interfere with the long-range macromolecular dynamics, causing some retardation of the relaxation processes,

while the short-range motions of the polymer chains are almost unaffected by the presence of the filler. Interestingly, a significant increase of the low-frequency complex viscosity is achieved for the composites containing 1 wt.% of ETC, while a further increment of the particle loading causes a less pronounced effect on the complex viscosity values. This finding can be explained considering that, due to the segregated morphology of the UHMWPE/ETC systems, the increase of particle loadings does not promote an increment of the polymer/particles interfacial area. More in detail, in the composites containing 1 wt.% of ETC, the formation of particle-rich channels occurs, inducing some restrains of the relaxation process of UHMWPE macromolecules and an increase of the low-frequency complex viscosity^{46,47}. The addition of higher amounts of ETC causes a modest rise of the complex viscosity, as the introduced particles contribute to the increase of the particle path thickness only.

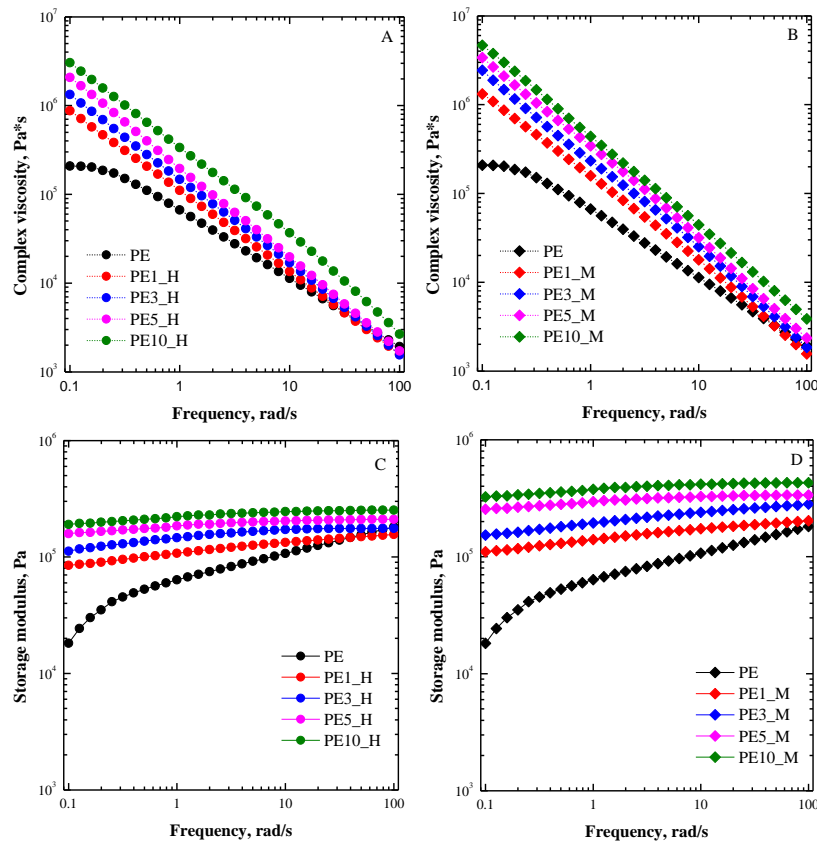


Figure 5. Complex viscosity curves (A and B) and storage modulus (C and D) as a function of frequency for UHMWPE and all UHMWPE/ETC composites.

To better evaluate the different effect of the two preparation methods on the composite rheological response, the dimensionless low-frequency complex viscosities (obtained as the ratio between the complex viscosity of the composite and that of the unfilled UHMWPE, both evaluated at 0.1 rad/s) were evaluated for both PEx_H and PEx_M systems; their trend as a function of the ETC loading is depicted in Figure 6. It is clearly noticeable that higher complex viscosity values are shown for PEx_M composites. Furthermore, it is worth noticing that the difference between the complex viscosity values of the two series of composites is more pronounced at high ETC contents.

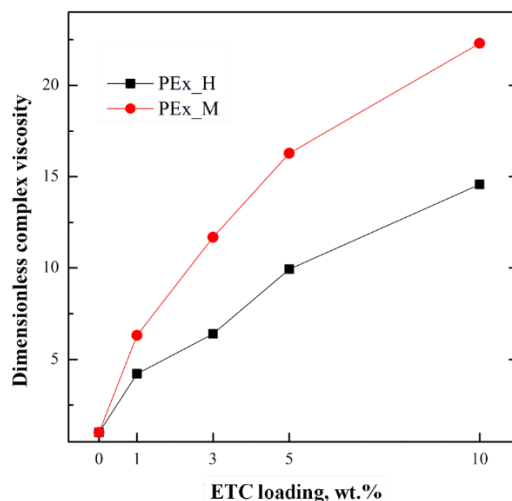


Figure 6. Dimensionless complex viscosity values (measured at 0.1 rad/s).

According to the morphological characterization, these findings can be associated with the higher effectiveness of the ball impact method in achieving a better distribution of the particles around the UHMWPE grains in the initial powder mixtures, resulting in the formation of a more regular microstructure, especially in the composites containing higher ETC amounts. In fact, the large particle agglomerates formed in PE_H composites limit the establishment of polymer/particle interactions, thus preventing the achievement of the high complex viscosity values achieved by the impact milled counterparts.

The Young modulus, stress and strain at break values of UHMWPE and its composites are depicted in the bar histograms of Figure 7. The presence 1 wt.% of ETC particles induces an increase of the Young modulus of UHMWPE. In particular, the composite obtained by impact mill (PE1_M) and by homogenizer (PE1_H), achieve Young modulus values higher than that of bare polymer by 50 and 18%, respectively. Beyond this loading, Young modulus of the composites obtained by homogenizer drops down and becomes lower than that of UHMWPE; conversely, it remains slightly higher for the composites prepared by impact mill. The stress at break of the composites remains almost unchanged, whereas the elongation at break is always lower than that of the unfilled polymer, as expected in reinforced composites ⁴⁸.

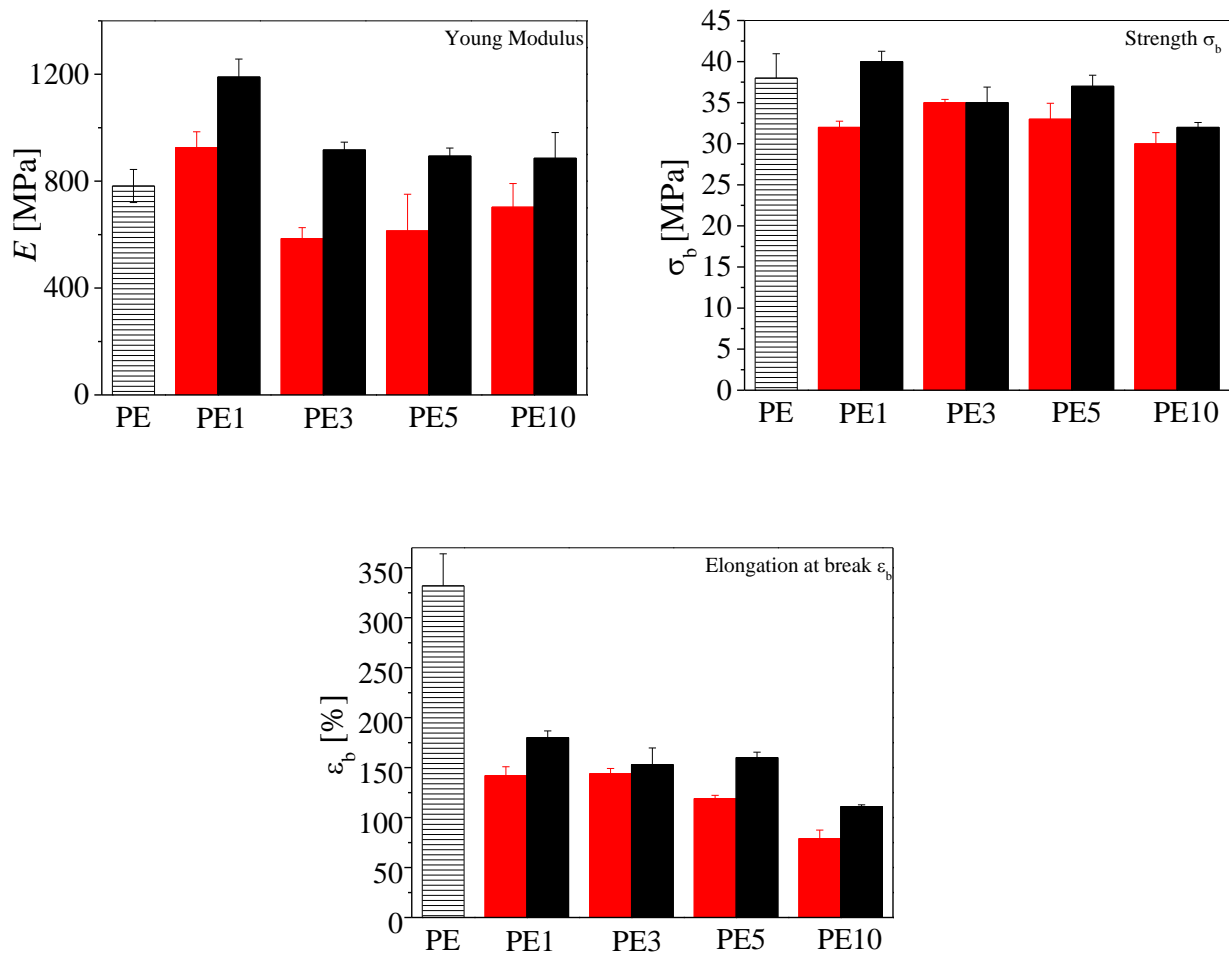


Figure 7. Mechanical parameters for UHMWPE and UHMWPE/ETC composites. Red and black bars are for PEx_H and PEx_M composites, respectively.

Interestingly, the mechanical parameters for impact milled composites are, generally, always higher than those measured for homogenized counterparts. This behavior can be ascribed to the better dispersion of ETC around the UHMWPE grains, as confirmed by optical, scanning electron microscopy and rheological analyses. The better dispersion is responsible for a more efficient transfer of the applied stress and for preventing the craze propagation ⁴⁸.

Table 1 collects the thermal conductivities of UHMWPE/ETC composites. In general, it can be observed that the addition of ETC has not a significant effect on the thermal conductivity of the composites obtained with the homogenizer (PE_x_H). Conversely, there is an enhancement in thermal conductivity for the composites prepared with the impact mill (PE_x_M). In fact, for these composites, the presence of ETC, irrespective of the loading, increases the value from 0.46 W/mK (unfilled UHMWPE) to about 0.55 W/mK. This behaviour can be ascribed to the different morphologies observed by SEM and POM for the two composites, due to the different powder mixing processes (i.e. homogenizer vs. impact mill) employed. In fact, in PE_x_H composites, ETC particles have a higher intra-particle distance due to the lower energy mixing process, with a lower number of interconnecting network, even at high filler loading, with respect to that found for the composites obtained by high energy impact milling. These results are reported also in other works ^{49,50} where it is stated that the good dispersion and formation of close packed structure are responsible for the improvement of the thermal conductivity.

Table 1. Thermal conductivity of UHMWPE/ETC composites.

	Thermal conductivity, W/mK	
	PE _x _H	PE _x -M
0	0.46±0.01	0.46±0.01
1	0.47±0.01	0.55±0.02
3	0.49±0.01	0.56±0.02
5	0.49±0.02	0.57±0.03
10	0.47±0.03	0.53±0.02
20	0.47±0.02	0.54±0.03

The electrical resistivity of UHMWPE/ETC composites as a function of ETC content is depicted in Figure 8. All the composites, irrespective of the preparation method, follow a classical electrical

percolation behaviour. As expected from an insulating material ⁵¹, unfilled UHMWPE exceeds the maximum measurable value with the instrumentation used in this work (i.e. $10^{18} \Omega \cdot \text{m}$). For the composites obtained by homogenizer, when the concentration is 1 wt.% or below this value (0.51 vol%), the composite is an insulator, as the ETC channels are not very well connected. Between 3 and 5 wt.% of ETC, electrical percolation occurs as a sudden decrease in electrical resistivity is observed.

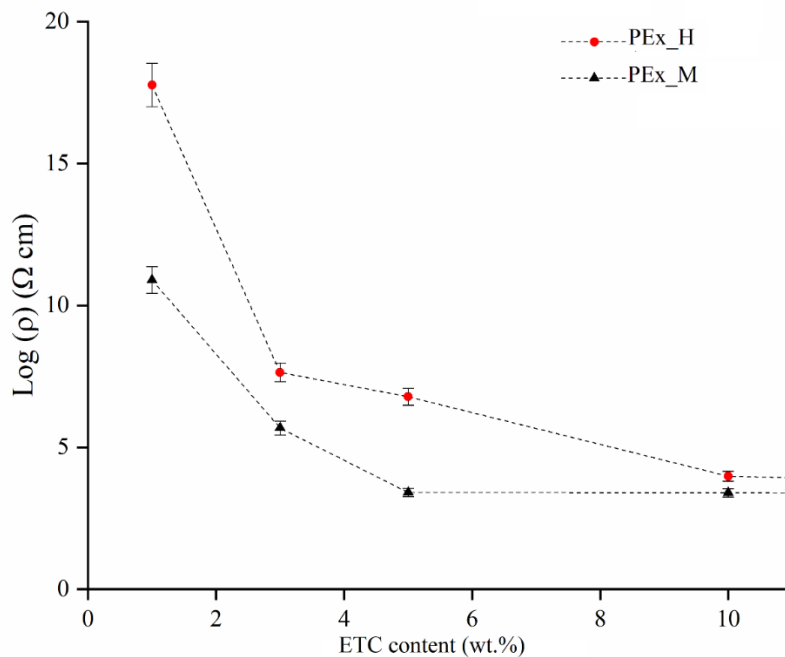


Figure 8. The electrical resistivity as a function of ETC content for composites obtained by homogenizer (PEx_H) and impact mill (PEx_M).

This is due to the formation of a conductive network that reduces the resistivity of about 11 orders of magnitude with respect to that of PE1_H (the volume resistivity is $4 \cdot 10^7 \Omega \cdot \text{cm}$ for PE3_H and $6 \cdot 10^6 \Omega \cdot \text{cm}$ for PE5_H, respectively). Though the value of electrical percolation found in this work is lower than that reported for other polymer composites obtained by compression molding ⁵², it is aligned with other values found for UHMWPE composites ³⁷. In particular, the electrical percolation is strictly related to the peculiar morphology of UHMWPE, whose powder particles during mixing and compression molding act as volume exclusion zones, forcing ETC particles to concentrate at the

external polymer surface. Beyond 5 wt.% of filler loading, the resistivity only slightly decreases reaching the value of $2.6 \cdot 10^3 \Omega \cdot \text{cm}$ when the amount of ETC is 10 wt.%.

A similar behaviour can be observed for the composites obtained by impact mill. However, for these composites, a volume resistivity of $7.8 \cdot 10^{10} \Omega \cdot \text{cm}$ is recorded when the amount of ETC is 1 wt.%. This value of resistivity is of about 7 order of magnitude lower respect to the composite obtained by homogenizer at the same filler loading. By increasing the amount of ETC, the electrical resistivity is always lower respect to that of PEx_H; conversely, at high loadings (i.e. 10 and 20 wt.%), it approaches that of the homogenized composites. The improved conductivity of PEx_M with respect to PEx_H can be ascribed to the better distribution of filler around grains and its close packed morphology that can influence the contact resistance between the adjacent ETC particles in the composites obtained by impact mill. At higher concentration, the intrinsic conductivity of the filler becomes predominant and no difference can be find in the related composites⁵³⁻⁵⁵.

The resistivity of the filler network was evaluated by using a statistical power law (eq.1), estimating the conductivity of the filler (eq.2) according to the following equations

$$\rho = \rho_f (v - v_p)^{-t} \quad (\text{eq.1})$$

$$\rho = \sigma^{-1} \quad (\text{eq.2})$$

where ρ is the volume resistivity of the composite, v is the volume fraction, v_p is the volume fraction at the percolation threshold, t is the critical exponent and σ is the conductivity. Considering the data reported in figure 8, the v_p is assumed to be 3 wt.% (1.52 vol.%) and the log-log plot based on eq.1 is shown in Figure 9.

The estimation of ρ_0 from the figure showed a value of 0.49 and 6.92 $\Omega \cdot \text{cm}$ for PEx_H and PEx_M respectively. Furthermore, the conductivity of the ETC network in the composites is equal to 2.09 S/m for PEx_H and to 0.15 S/m for PEx_M. These values clearly show a better electronic performances of the ETC network in PEx_H systems. This is reasonably due to the more heterogeneous dispersion of the filler in PEx_H rather than PEx_M samples, with the formation of highly dense regions as shown in figure 3. As a consequence, PEx_M showed a more clear percolation

threshold, while the highly filled region present in PEx_H boosted the ETC network conductivity to high filler loadings, improving the electrons mobility. This is supported also by the value of t that was quite close to the theoretical value of 2 as reported by Nakamura⁵⁶, whereas the impact milling procedure causes an evident decrease.

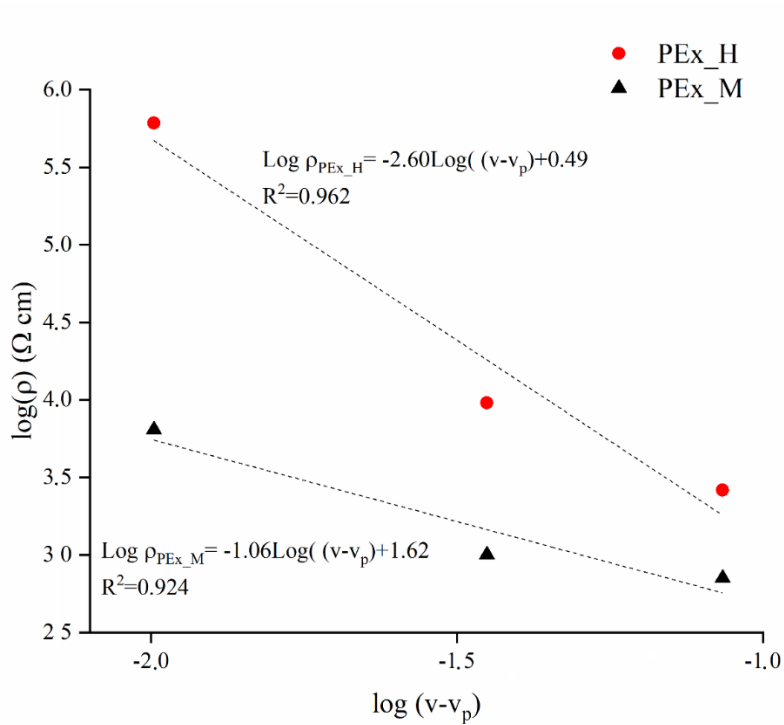


Figure 9. Statistical power law log-log fitting for PEx-H and PEx_M for $v > v_p$.

In literature, the small values of t were not interpreted on the basis of a dimensionality reduction⁵⁷, but were ascribed to aggregation of filler particles, their mutual attraction, or activated hopping transfer mechanism of the conductivity⁵⁸. From a general point of view, considering both the trends of electric and mechanical properties, it is reasonably assumed a better filler-polymer grain interaction in the case of PEx_M and a better filler-filler interaction for PEx_H.

4. Conclusions

In this work, we have prepared ultra high molecular weight polyethylene based composites containing exhausted tire carbon as alternative to expensive and non-sustainable carbonaceous fillers. Two

techniques were employed for mechanically mixing the powder components, i.e. a homogenizer and a home-made impact mill; the mixing step was followed by compression molding.

The mixing methods affected the rheological and morphological features of the composites that, in turn, influenced their mechanical, thermal and electrical behavior. Better performances were achieved for the composites obtained with the impact mill, which showed improved Young modulus, reduced electrical and thermal resistance with respect to homogenized counterparts. The results were ascribed to the better distribution of filler and close packed filler around the polymer grains that influenced the contact between the adjacent ETC particles in the composites obtained by impact mill. From a general point of view, it was demonstrated that ETC has great potential as a filler for polymers in a variety of electrical and engineering applications.

References

1. Nadal M, Rovira J, Díaz-Ferrero J, Schuhmacher M, Domingo JL. Human exposure to environmental pollutants after a tire landfill fire in Spain: Health risks. *Environment international*. 2016;97:37-44.
2. Singh A, Spak SN, Stone EA, et al. Uncontrolled combustion of shredded tires in a landfill—Part 2: Population exposure, public health response, and an air quality index for urban fires. *Atmospheric Environment*. 2015;104:273-283.
3. Pettinao E, Navach S, Cesaretti D, Leoni S. *L'Italia del Riciclo*. Italy: FONDAZIONE PER LO SVILUPPO SOSTENIBILE (FISE UNIRE), Unione Nazionale Imprese Recupero;2011.
4. Presti DL. Recycled tyre rubber modified bitumens for road asphalt mixtures: A literature review. *Construction and Building Materials*. 2013;49:863-881.
5. Gupta T, Siddique S, Sharma RK, Chaudhary S. Behaviour of waste rubber powder and hybrid rubber concrete in aggressive environment. *Construction and Building Materials*. 2019;217:283-291.

6. Záleská M, Pavlík Z, Čítek D, Jankovský O, Pavlíková M. Eco-friendly concrete with scrap-tyre-rubber-based aggregate—Properties and thermal stability. *Construction and Building Materials*. 2019;225:709-722.
7. Banaszekiewicz K, Badura M. Experimental investigation on the application of recycled tires polymer fibers as a BTEX removal material. *SN Applied Sciences*. 2019;1(6):1-10.
8. Sunthonpagasit N, Duffey MR. Scrap tires to crumb rubber: feasibility analysis for processing facilities. *Resources, Conservation and Recycling*. 2004;40(4):281-299.
9. Schmidt M, Spieth H, Haubach C, Kühne C. Material flow cost accounting in variant production. In 100 Pioneers in Efficient Resource Management. In: Springer: Berlin/Heidelberg, Germany; 2019.
10. Quadrini F, Santo L, Musacchi E. A sustainable molding process for new rubber products from tire recycling. *Progress in Rubber, Plastics and Recycling Technology*. 2019;35(1):41-55.
11. Antoniou NA, Zorpas AA. Quality protocol and procedure development to define end-of-waste criteria for tire pyrolysis oil in the framework of circular economy strategy. *Waste Management*. 2019;95:161-170.
12. Antoniou N, Zabaniotou A. Re-designing a viable ELTs depolymerization in circular economy: Pyrolysis prototype demonstration at TRL 7, with energy optimization and carbonaceous materials production. *Journal of cleaner production*. 2018;174:74-86.
13. Martínez JD, Puy N, Murillo R, García T, Navarro MV, Mastral AM. Waste tyre pyrolysis—A review. *Renewable and sustainable energy reviews*. 2013;23:179-213.
14. Lee N, Joo J, Lin K-YA, Lee J. Thermochemical conversion of mulching film waste via pyrolysis with the addition of cattle excreta. *Journal of Environmental Chemical Engineering*. 2021;9(6):106362.
15. Sathiskumar C, Karthikeyan S. Recycling of waste tires and its energy storage application of by-products—a review. *Sustainable Materials and Technologies*. 2019;22:e00125.

16. Martínez JD, Veses A, Mastral AM, et al. Co-pyrolysis of biomass with waste tyres: Upgrading of liquid bio-fuel. *Fuel Processing Technology*. 2014;119:263-271.
17. Nisar J, Ali G, Ullah N, et al. Pyrolysis of waste tire rubber: Influence of temperature on pyrolysates yield. *Journal of Environmental Chemical Engineering*. 2018;6(2):3469-3473.
18. Nkosi N, Muzenda E, Gorimbo J, Belaid M. Developments in waste tyre thermochemical conversion processes: gasification, pyrolysis and liquefaction. *RSC Advances*. 2021;11(20):11844-11871.
19. Mavukwana A-e, Stacey N, Fox JA, Sempuga BC. Thermodynamic comparison of pyrolysis and gasification of waste tyres. *Journal of Environmental Chemical Engineering*. 2021;9(2):105163.
20. Berki P, Karger-Kocsis J. Comparative properties of styrene-butadiene rubbers (SBR) containing pyrolytic carbon black, conventional carbon black, and organoclay. *Journal of Macromolecular Science, Part B*. 2016;55(7):749-763.
21. Martínez JD, Cardona-Uribe N, Murillo R, García T, López JM. Carbon black recovery from waste tire pyrolysis by demineralization: Production and application in rubber compounding. *Waste management*. 2019;85:574-584.
22. Dimpe KM, Ngila JC, Nomngongo PN. Application of waste tyre-based activated carbon for the removal of heavy metals in wastewater. *Cogent Engineering*. 2017;4(1):1330912.
23. Kumar R, Sharma A. Morphologically tailored activated carbon derived from waste tires as high-performance anode for Li-ion battery. *Journal of Applied Electrochemistry*. 2018;48(1):1-13.
24. Naskar AK, Bi Z, Li Y, et al. Tailored recovery of carbons from waste tires for enhanced performance as anodes in lithium-ion batteries. *Rsc Advances*. 2014;4(72):38213-38221.
25. Li Y, Paranthaman MP, Akato K, et al. Tire-derived carbon composite anodes for sodium-ion batteries. *Journal of Power Sources*. 2016;316:232-238.

26. Hood ZD, Yang X, Li Y, Naskar AK, Chi M, Paranthaman MP. Conversion of waste tire rubber into high-value-added carbon supports for electrocatalysis. *Journal of the Electrochemical Society*. 2018;165(14):H881.
27. Chen W, Feng H, Shen D, et al. Carbon materials derived from waste tires as high-performance anodes in microbial fuel cells. *Science of the Total Environment*. 2018;618:804-809.
28. Zhao P, Han Y, Dong X, Zhang C, Liu S. Application of activated carbons derived from scrap tires as electrode materials for supercapacitors. *ECS Journal of Solid State Science and Technology*. 2015;4(7):M35.
29. Urrego-Yepes W, Cardona-Urbe N, Vargas-Isaza CA, Martínez JD. Incorporating the recovered carbon black produced in an industrial-scale waste tire pyrolysis plant into a natural rubber formulation. *Journal of Environmental Management*. 2021;287:112292.
30. Verma A, Baurai K, Sanjay M, Siengchin S. Mechanical, microstructural, and thermal characterization insights of pyrolyzed carbon black from waste tires reinforced epoxy nanocomposites for coating application. *Polymer Composites*. 2020;41(1):338-349.
31. Spiegelberg S, Kozak A, Braithwaite G. Characterization of physical, chemical, and mechanical properties of UHMWPE. In: *UHMWPE Biomaterials Handbook*. Elsevier; 2016:531-552.
32. Lisunova M, Mamunya YP, Lebovka N, Melezhyk A. Percolation behaviour of ultrahigh molecular weight polyethylene/multi-walled carbon nanotubes composites. *European Polymer Journal*. 2007;43(3):949-958.
33. Pang H, Chen C, Bao Y, et al. Electrically conductive carbon nanotube/ultrahigh molecular weight polyethylene composites with segregated and double percolated structure. *Materials Letters*. 2012;79:96-99.

34. Hu H, Zhang G, Xiao L, Wang H, Zhang Q, Zhao Z. Preparation and electrical conductivity of graphene/ultrahigh molecular weight polyethylene composites with a segregated structure. *Carbon*. 2012;50(12):4596-4599.
35. Wang B, Li H, Li L, Chen P, Wang Z, Gu Q. Electrostatic adsorption method for preparing electrically conducting ultrahigh molecular weight polyethylene/graphene nanosheets composites with a segregated network. *Composites Science and Technology*. 2013;89:180-185.
36. Li S, Xu Y, Jing X, Yilmaz G, Li D, Turng L-S. Effect of carbonization temperature on mechanical properties and biocompatibility of biochar/ultra-high molecular weight polyethylene composites. *Composites Part B: Engineering*. 2020;196:108120.
37. Li S, Li X, Chen C, et al. Development of electrically conductive nano bamboo charcoal/ultra-high molecular weight polyethylene composites with a segregated network. *Composites Science and Technology*. 2016;132:31-37.
38. Li S, Li X, Deng Q, Li D. Three kinds of charcoal powder reinforced ultra-high molecular weight polyethylene composites with excellent mechanical and electrical properties. *Materials & Design*. 2015;85:54-59.
39. Duraccio D, Strongone V, Faga M, et al. The role of different dry-mixing techniques on the mechanical and biological behavior of UHMWPE/alumina-zirconia composites for biomedical applications. *European Polymer Journal*. 2019;120:109274.
40. Tagliaferro A, Rovere M, Padovano E, Bartoli M, Giorcelli M. Introducing the Novel Mixed Gaussian-Lorentzian Lineshape in the Analysis of the Raman Signal of Biochar. *Nanomaterials*. 2020;10(9):1748.
41. Giorcelli M, Bartoli M. Development of Coffee Biochar Filler for the Production of Electrical Conductive Reinforced Plastic. *Polymers*. 2019;11(12):17.

42. Gustavsson M, Karawacki E, Gustafsson SE. Thermal conductivity, thermal diffusivity, and specific heat of thin samples from transient measurements with hot disk sensors. *Review of Scientific Instruments*. 1994;65(12):3856-3859.
43. Blythe AR. Electrical resistivity measurements of polymer materials. *Polymer Testing*. 1984;4(2):195-209.
44. Tamborrino V, Costamagna G, Bartoli M, et al. Catalytic oxidative desulphurization of pyrolytic oils to fuels over different waste derived carbon-based catalysts. *Fuel*. 2021;296:120693.
45. Ferrari AC, Robertson J. Interpretation of Raman spectra of disordered and amorphous carbon. *Physical review B*. 2000;61(20):14095.
46. Zhang X, Tan Y, Li Y, Zhang G. Effect of OMMT on microstructure, crystallisation and rheological behaviour of UHMWPE/PP nanocomposites under elongation flow. *Plastics, Rubber and Composites*. 2018;47(7):315-323.
47. Zhao L, Xia W, Zhang P. Economical conductive graphite-filled polymer composites via adjustable segregated structures: Construction, low percolation threshold, and positive temperature coefficient effect. *Journal of Applied Polymer Science*. 2021;138(17):50295.
48. Duraccio D, Strongone V, Malucelli G, et al. The role of alumina-zirconia loading on the mechanical and biological properties of UHMWPE for biomedical applications. *Composites Part B: Engineering*. 2019;164:800-808.
49. Lee G-W, Park M, Kim J, Lee JI, Yoon HG. Enhanced thermal conductivity of polymer composites filled with hybrid filler. *Composites Part A: Applied Science and Manufacturing*. 2006;37(5):727-734.
50. Samad MA, Sinha SK. Mechanical, thermal and tribological characterization of a UHMWPE film reinforced with carbon nanotubes coated on steel. *Tribology International*. 2011;44(12):1932-1941.

51. Zhang C, Ma C-A, Wang P, Sumita M. Temperature dependence of electrical resistivity for carbon black filled ultra-high molecular weight polyethylene composites prepared by hot compaction. *Carbon*. 2005;43(12):2544-2553.
52. Sumita M, Takenaka K, Asai S. Characterization of dispersion and percolation of filled polymers: molding time and temperature dependence of percolation time in carbon black filled low density polyethylene. *Composite Interfaces*. 1995;3(3):253-262.
53. Rahaman M, Chaki TK, Khastgir D. Modeling of DC conductivity for ethylene vinyl acetate (EVA)/polyaniline conductive composites prepared through insitu polymerization of aniline in EVA matrix. *Composites Science and Technology*. 2012;72(13):1575-1580.
54. Thongruang W, Spontak RJ, Balik CM. Correlated electrical conductivity and mechanical property analysis of high-density polyethylene filled with graphite and carbon fiber. *Polymer*. 2002;43(8):2279-2286.
55. Shui X, Chung DDL. Submicron diameter nickel filaments and their polymer-matrix composites. *Journal of Materials Science*. 2000;35(7):1773-1785.
56. Nakamura S, Saito K, Sawa G, Kitagawa K. Percolation threshold of carbon black-polyethylene composites. *Japanese journal of applied physics*. 1997;36(8R):5163.
57. Sandler J, Kirk J, Kinloch I, Shaffer M, Windle A. Ultra-low electrical percolation threshold in carbon-nanotube-epoxy composites. *Polymer*. 2003;44(19):5893-5899.
58. Kilbride Be, Coleman J, Fraysse J, et al. Experimental observation of scaling laws for alternating current and direct current conductivity in polymer-carbon nanotube composite thin films. *Journal of applied physics*. 2002;92(7):4024-4030.